J. Physiol. (1987), **384**, *pp.* 49–79
With 12 text-figures
Printed in Great Britain

THE RECEPTIVE-FIELD SPATIAL STRUCTURE OF CAT RETINAL Y CELLS

BY CHRISTINA ENROTH-CUGELL AND ALAN W. FREEMAN*

From the Biomedical Engineering Division, Technological Institute, Northwestern University, Evanston, IL 60201, U.S.A.

(*Received 21 March 1986*)

SUMMARY

1. Y-type ganglion cells in the cat's retina were stimulated with bars of light and grating patterns at photopic luminances. Stimuli were stationary, and luminance at each point was varied sinusoidally in time at 2 Hz. Impulse rates were recorded from single cells.

2. When the stimulus was a narrow bar of light, the impulse rate approached a sinusoidal function of time as contrast was reduced. The linear behaviour of each cell was therefore characterized by taking the limit of response parameters as contrast approached zero.

3. The ratio of surround strength to centre strength varied widely between cells but the two strengths were approximately equal on average. The difference between surround phase and centre phase averaged 168 deg.

4. As contrast increased, responses became rectified. Rectifier output was well described by a power law of stimulus amplitude, where the power was usually 1·4 or 1·5.

5. Response phase advanced with increasing contrast, and at high response amplitudes grew less than proportionally with contrast. These effects were assumed due to the contrast gain control described by Shapley & Victor (1978).

6. Gratings in which luminance varied sinusoidally with distance were used to determine Y cell spatial resolution. The second-harmonic amplitude of the response diminished rapidly with increasing spatial frequency: the radius of the best-fitting Gaussian mechanism was about 0·25 deg for a cell at 10 deg eccentricity.

7. This spatial resolution is close to the linear resolution of X cells as determined by Linsenmeier, Frishman, Jakiela & Enroth-Cugell (1982).

8. A receptive field model incorporating both linear and non-linear elements is described. The model consists of an array of subunit pathways, each of which has a centre–surround organization followed by a rectifier; a pool weights and sums subunit outputs, and signals are then passed through a contrast gain control.

9. The model accounts qualitatively for the over-all centre–surround organization of Y cell linear responses, the dependence of frequency-doubled responses on spatial frequency, and impulse rate as a function of time for a variety of bar and grating stimuli.

* To whom all reprint requests should be sent: Physiology Department F13, University of Sydney, NSW 2006, Australia.

INTRODUCTION

It is clear that non-linearities play an essential role in visual function. Adaptation, for instance, is an inherently non-linear process since it involves a change in the sensitivity of the visual system when the ambient level of illumination changes. The subject of this paper is a population of cells in the retina, Y-type ganglion cells, which operate in a characteristically non-linear fashion on the visual stimulus. The Y cell was first distinguished from other ganglion cell types by a test which shows that signals from one part of its receptive field cannot be made to cancel signals from another part, regardless of the spatial configuration of the stimulus (Enroth-Cugell & Robson, 1966). Another expression of non-linearity in Y cell function is the contrast gain control described by Shapley & Victor (1978). At low temporal frequencies, this mechanism results in response amplitudes that grow less than proportionally, and in advancing phase, with increasing contrast.

Given the importance of non-linear processes for vision, it is desirable to know how the Y cell operates. Previous studies (e.g. Enroth-Cugell & Robson, 1966; Cleland, Dubin & Levick, 1971; Linsenmeier *et al.* 1982; Derrington & Lennie, 1982), particularly those of Shapley and his colleagues (e.g. Hochstein & Shapley, 1976*a*, *b*; Shapley & Victor, 1978; Victor & Shapley, 1979; Shapley & Victor, 1981), have described various facets of contrast processing in Y cells. It cannot be said, however, that contrast processing in this population of cells is completely, or even well, understood. If it were, it would be possible to predict the response of a Y cell to an arbitrary spatiotemporal pattern of luminance on the retina. Current knowledge of Y cell mechanisms, however, is not sufficient to attempt such a synthesis. Our aim in this paper is to use existing data and new observations to construct a model for spatial mechanisms in the Y cell receptive field at low temporal frequency and a photopic adaptation level. Further, we aim to show that this model can qualitatively account for the response of a Y cell to a limited set of spatial patterns under these experimental conditions.

A preliminary report of this work has been published (Freeman & Enroth-Cugell, 1985).

METHODS

Animal preparation. Adult cats were anaesthetized with halothane while two venous catheters were inserted. One catheter was used for infusing anaesthetics: sodium thiamylal was used until preparatory surgery was completed, and urethane thereafter. The loading dose for the latter was 200 mg kg^{-1}, while the steady infusion rate, 20–30 mg kg^{-1} h^{-1}, was more than six times higher than one that maintains light anaesthesia in unparalysed cats (Cleland & Enroth-Cugell, 1966), and about the same as that used in a recent study of paralysed animals (Enroth-Cugell, Robson, Schweitzer-Tong & Watson, 1983). Heart rate and blood pressure were carefully monitored for changes that may be associated with painful stimuli; if such changes occurred, the urethane infusion rate was increased. The other catheter was used to infuse 20–30 mg gallamine triethiodide kg^{-1} h^{-1}; together with bilateral transection of the cervical sympathetic trunk, this minimized eye movements. Respiratory stroke volume was adjusted to maintain end-tidal CO_2 at 4 %, rectal temperature was kept at 39 °C. Locally applied phenylephrine and atropine retracted the nicitating membranes, and dilated the pupils, respectively. Contact lenses with 4 mm diameter pupils were fitted to both eyes. Electrical recordings from the right optic tract were made with glass-insulated tungsten microelectrodes.

Stimulation. Stimuli were presented on a cathode-ray tube with a P31 phosphor (Joyce Electronics, Cambridge, U.K.). The tube face measured 31 cm horizontally by 21 cm vertically and was placed 114 cm from the cat so that it subtended 16×10 deg. The raster stimulus was composed of thirty lines per degree of visual angle, and was presented at 160 frames s^{-1}. Mean luminance was fixed at 420 cd m^{-2}; with 4 mm diameter pupils, this produces a retinal illumination in the photopic range (Enroth-Cugell, Hertz & Lennie, 1977). One-dimensional spatial patterns were generated on the tube face by holding the luminance constant along an individual raster line, but varying the luminance from line to line. During each frame, line luminances were read from a digital-to-analogue converter (d.a.c.) with memory (Cambridge Electronic Design, Cambridge, U.K.) in which the required spatial pattern had been previously stored. Lines ran vertically, so that the displayed pattern was modulated horizontally. Temporal variation in the stimulus was obtained by multiplying the signal from the memory d.a.c. by the output of another d.a.c.; the signal from the second d.a.c. was constant during a frame, but varied from frame to frame. For the bar and grating stimuli described in the Results section, the temporal wave form used was a 2 Hz sinusoid. Contrast was determined by subtracting the mean luminance from the maximum luminance in a temporal cycle, and dividing that difference by mean luminance. The highest contrast used was 0·9.

Experimental protocol. At the beginning of a recording session, the visual stimulus was focused on both retinas by placing spherical spectacle lenses in front of the eyes. Lens powers were adjusted to obtain the maximum response from a ganglion cell to a high spatial frequency grating presented on the cathode-ray-tube face. A reference map for plotting receptive-field locations was produced by illuminating the retina via a fibre-optic light guide held at the cornea. The reflected image of the optic disk and blood vessels was then drawn on a tangent screen. The location of the area centralis (relative to the disk) was estimated by the method of Nikara, Bishop & Pettigrew (1968), and receptive field eccentricity measured from the point so determined. After obtaining the eccentricity of a unit, a mirror in front of the cat was used to image the face of the cathode-ray tube on the retina. A *contrast-reversing* edge stimulus on the tube face, that is, a stationary edge stimulus for which luminance at each point varied sinusoidally in time, was centred over the receptive field by turning the mirror until the linear component of the response was reduced to zero.

The coarseness of the electrodes used here (tip length greater than 10 μm) biased against the recording of cells with thin axons. It can therefore be safely assumed that cells fell into the X and Y ganglion cell categories of Enroth-Cugell & Robson (1966), or equivalently, the *brisk* category of Cleland & Levick (1974). X and Y cells were distinguished by stimulating each cell with a 1 cycle deg^{-1} sinusoidal grating successively presented at a number of spatial phases distributed evenly across half a spatial cycle. The grating was stationary and contrast-reversed at 4 or 8 Hz. A sinusoidal function of stimulus spatial phase was fitted to the fundamental Fourier response amplitude, while the amplitude of the second harmonic was averaged across phases (Hochstein & Shapley, 1976*a*). Cells were classified as Y-type when the second-harmonic amplitude determined in this way exceeded the fundamental amplitude. One cell (0602) that failed this test is also included; for this cell the ratio of second-harmonic amplitude to fundamental amplitude was 0·9, but the radius of its centre mechanism (1·25 deg at 28·7 deg eccentricity) indicated classification as Y-type (see Linsenmeier *et al.* 1982).

A correction for eye movements was made while recording from each cell. Every 10 to 15 min, a 0·25 deg wide bar was slowly swept five times across the receptive field, and the impulse rate computed as a function of time during a sweep. The result was compared with the time course obtained in the same way immediately following the centring and classification of the receptive field. A shift in the response peak to either side was interpreted as due to eye movements, and stimuli delivered thereafter were shifted by the amount required to compensate for the eye movements.

Data collection and analysis. Impulse occurrence times from single cells were detected with a trigger circuit, and interimpulse intervals recorded digitally with a resolution of 10 μs. Data collection periods were organized into trials of 7 s or longer in length. Stimuli were presented for at least a second before the beginning of a trial to allow the cell's activity to stabilize. For each spatial configuration of a stimulus, at least four contrast levels were used. The contrasts were chosen to be multiples (1, 2, 3,...) of the contrast that yielded a root mean square variation of impulse rate about the mean rate of approximately 5 impulses s^{-1}. All stimuli were periodic in time, and the response could therefore be characterized with a Fourier series. The amplitude and phase of

the first eight Fourier components of the impulse rate were computed for each trial by convolving sine and cosine functions of time with a series of delta functions representing the impulse train. Impulse rate as a function of time during the stimulus cycle was determined in two steps. First, the Fourier series representing the frequency-domain response was multiplied by a Gaussian spectrum that reduced the eighth harmonic to 13 % of its original amplitude; multiplication by this Gaussian spectrum in the frequency domain is equivalent to smoothing in the time domain using a temporal Gaussian profile with a standard deviation of 0·04 stimulus cycles. Secondly, an inverse Fourier transformation was performed to obtain the time-domain response. The frequency-domain procedure used here avoids the loss of temporal resolution inherent in a binning method.

Terminology. The term *responsivity* is used for the amplitude of the fundamental Fourier response component divided by contrast (Enroth-Cugell *et al.* 1983). We use impulses s^{-1} contrast-unit^{-1} (rather than impulses s^{-1}) as its unit to help distinguish between responsivity and the amplitude of the fundamental. Response phase is measured as the difference between the phase of the fundamental Fourier component and that of the stimulus, in units of degrees. The *responsivity vector* is the vector with magnitude equal to the responsivity, and with the phase of the response. Since all stimuli were periodic, the phase relationship between any two signals evoked by a stimulus (for instance, the centre and surround signals described below) can be given as a specific number of degrees to which is added an arbitrary integral multiple of 360 deg. We therefore avoid the statement that one signal leads or lags another signal, specifying instead the phase difference between the two signals; the phase value used is that which lies between −180 and 180 deg.

Gaussian centre–surround model. The Gaussian centre–surround model used here to describe the linear spatial characteristics of the Y cell receptive field is functionally identical to that used by Enroth-Cugell *et al.* (1983), with some differences in conventions. Briefly, the model's response is defined to be a vector (or equivalently, a complex number) since it has both magnitude and phase. The model's responsivity vector is assumed to be the sum of two other vectors, the signals from the centre and surround mechanisms. (The centre and surround signals that best fit experimental results at low temporal frequency are nearly out of phase, so the vector sum approximates a difference of scalars.) Each of the two mechanisms is described by three parameters: (1) the radius of the Gaussian function giving the mechanism's amplitude at each spatial location; (2) a strength, which is the fundamental amplitude of the signal evoked in that mechanism per unit of contrast of a spatially uniform stimulus covering the receptive field; (3) the temporal phase shift of the mechanism's signal relative to the stimulus. Since centring of the receptive field on the cathode-ray-tube face during an experiment was rarely exact, a seventh parameter, the location of the receptive field middle, is included here. These seven parameters were estimated for each cell by placing narrow contrast-reversing bars of width, b, at a number of locations, x, across the receptive field and recording the fundamental amplitude and phase of the cell's response at each location. From the quotient $F_P(w)/c$ in eqn. (21) of the Appendix, the model's responsivity vector is

$$R_g(x) = S_c \,\mathrm{erfb}(x-x_0, b, r_c) + S_s \,\mathrm{erfb}(x-x_0, b, r_s), \quad (1)$$

where erfb is a difference of error functions defined in the Appendix, S_c and S_s are vectors giving the centre's strength and phase and surround's strength and phase, r_c and r_s are the radii of the centre and surround mechanisms, and x_0 is the location of the receptive field middle. The model was fitted to the experimental data, and parameters estimated, in two steps. First, the radii r_c and r_s and the location x_0 were assigned fixed values. The error vector between model and experimental data was defined to be the difference between the cell's and the model's responsivity vectors, divided by a weighting proportional to the standard deviation of the measurement, the cell's responsivity (Enroth-Cugell *et al.* 1983). Eqn. (1), a linear regression equation in the vector parameters S_c and S_s, was then solved by choosing those parameter values that minimized the sum of squared error magnitudes across bar placements. Secondly, r_c, r_s and x_0 were varied within the ranges in which they were most likely to fall, and the linear regression performed for each combination. The combination that gave the minimum error not only provided estimates for r_c, r_s and x_0 but also for the vectors S_c and S_s.

RESULTS

The data were collected from thirteen on-centre and three off-centre Y cells from ten cats. We first describe the Y cell response to a spatially localized stimulus, and

to a grating stimulus. These experimental observations are then used to construct a model for the receptive-field spatial structure.

Responses to spatially localized stimuli

The stimuli used in the first part of the study were stationary, vertical, contrast-reversing bars presented against an otherwise uniform field. Bars were 10 deg long, usually 0·25 deg wide, and bar luminance varied sinusoidally at 2 Hz about the mean luminance of the whole screen. Fig. 1 shows the responses of two on-centre cells and one off-centre cell to a bar placed close to the receptive-field middle, and the responses when the stimulus was placed well away from the middle. Impulse rate (calculated by the procedure described in the Methods section) is plotted as a function of time during a stimulus cycle. Responses to five stimulus contrasts at each receptive-field location are shown. Several features of these responses are to be noted. First, when the stimulus is sinusoidally modulated in time, the response can deviate significantly from a sinusoidal function of time. In particular, at the higher response amplitudes, impulse rate during one-half of the stimulus cycle increases much more than it drops during the remainder of the cycle. This process of rectification, an aspect of Y cell non-linearity, can occur whether the bar is situated at the receptive-field middle or away from it. Secondly, at low response amplitudes, the impulse rate approximates a sinusoidal function of time. Thus the signal pathway approaches linear behaviour as contrast is reduced. The third feature of interest in Fig. 1 is the response phase. When the receptive field is stimulated at low contrasts at its middle, firing rate increases more or less in phase with the increase in bar luminance for the on-centre cells. For stimulation away from the middle, the response is shifted by approximately half a stimulus cycle, a reflexion of centre–surround organization. The off-centre cell is approximately half a cycle out of phase with the on-centre cells. Finally, equal contrast increments do not result in equal response increments: at high response amplitudes the response increments are smaller than at low amplitudes. Also, increasing contrast tends to advance response phase. Shapley & Victor (1978) described a *contrast gain control* which was responsible for reducing response increments and for advancing phase at low temporal frequencies (such as 2 Hz) and high contrast. The contrast gain control is assumed to be responsible for the effects seen here.

Non-linear aspects of the response

Fig. 2 shows the effect of the contrast gain control on the fundamental Fourier response component. The symbols give the amplitude and phase of the fundamental component as a function of contrast for two bar placements on the receptive fields of two on-centre cells. The fitting of the curves to these points will be described below. For a linear system, the fundamental amplitude would grow linearly and the phase would stay constant as contrast increased. The experimental data show that the fundamental amplitude of the response grows but the gradient decreases with increasing contrast, while the phase of the fundamental component advances with increasing contrast. These were standard findings across all the cells examined.

There is a non-linear aspect of the responses in Fig. 1 that is evident not only with increasing contrast, but also at a fixed contrast: positive-going excursions of impulse rate are greater than negative-going excursions. To explore the form of this

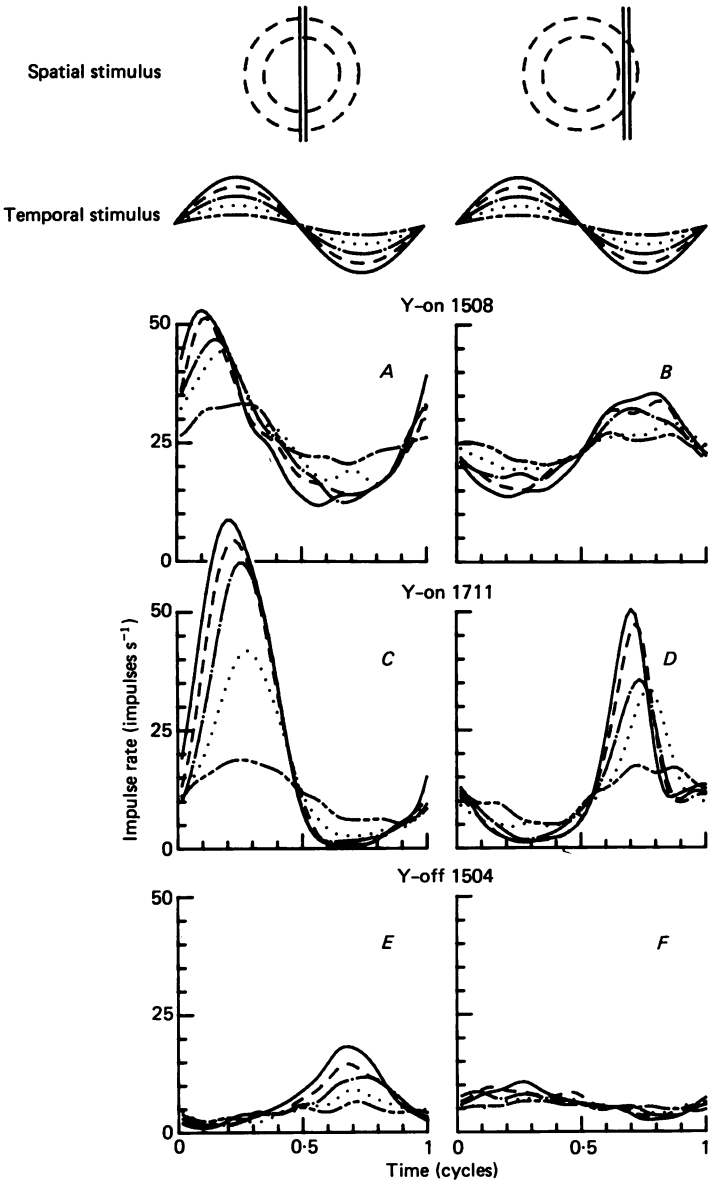

Fig. 1. Impulse rate profiles for a bar stimulus. The luminance of a thin (0·25 deg) bar of light was modulated about an otherwise uniform field of fixed luminance (420 cd m^{-2}). The bar was placed at the middle and outer receptive field, as shown at the top of the Figure; the inner and outer dashed circles have radii that roughly approximate the centre and surround radii, respectively, of a Y cell. The distance of the bar's mid-point from the middle of the receptive field was: *B*, 2·5 deg; *D*, 2·5 deg; and *F*, 2 deg. Bar luminance was a sinusoidal function of time, as shown by the wave form below the circles. Temporal frequency was 2 Hz. Five contrasts (shown by dashed lines of different types) were presented at each bar placement for each of the three cells. The contrasts were integral multiples (1, 2, 3, 4 and 5) of the following minimum contrasts: *A*, 0·05; *B*, 0·16; *C*, 0·03; *D*, 0·16; *E*, 0·05; and *F*, 0·16. The data collection period was 60 s at each contrast.

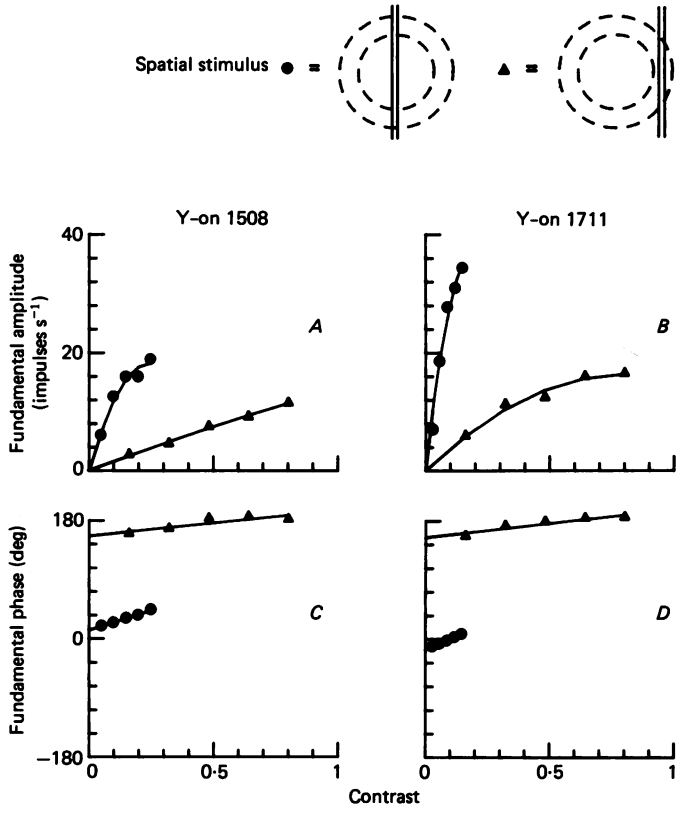

Fig. 2. The effect of contrast on the fundamental response component. Fourier components were determined for the responses of the on-centre cells shown in Fig. 1. Fundamental amplitude and phase are shown as functions of contrast when a contrast-reversing bar is placed at the middle (circles) and outer (triangles) receptive field. The curves through the experimentally determined points are the results of a least-squares linear regression in which the model was a quadratic function of contrast for the amplitude data, and a linear function for the phase data.

non-linearity it is useful to plot the Y cell's output (impulse rate) at each instant of time during a stimulus cycle against its input (instantaneous stimulus amplitude) at the same instant. Fig. 3*A* and *B*, replots of the data in Fig. 1*A*, are of this form, with one difference. Impulse rate is plotted against the instantaneous value of the fundamental response component, rather than against instantaneous stimulus amplitude, since the contrast gain control affects both impulse rate and its fundamental component in a similar fashion; plotting one against the other therefore reduces the effect of the contrast gain control on the plotted results. In Fig. 3*A*, results at different contrasts have been displaced vertically by arbitrary amounts to show the form of the individual curves; curves in Fig. 3*B* have not been shifted. Each curve in Fig.3*A* has two arms, one traced as impulse rate increases to its maximum value during a cycle (continuous line), the other traced as impulse rate decreases from the maximum (dashed line). If the non-linearity whose form is illustrated in the figure

were static, the two arms would superpose (a static non-linearity is one for which output at a particular time depends only on input at that time, and not at any other time), and the curves obtained at different contrasts would also superpose. Since there is approximate superposition in Fig. 3*B*, it appears that the signal pathway from

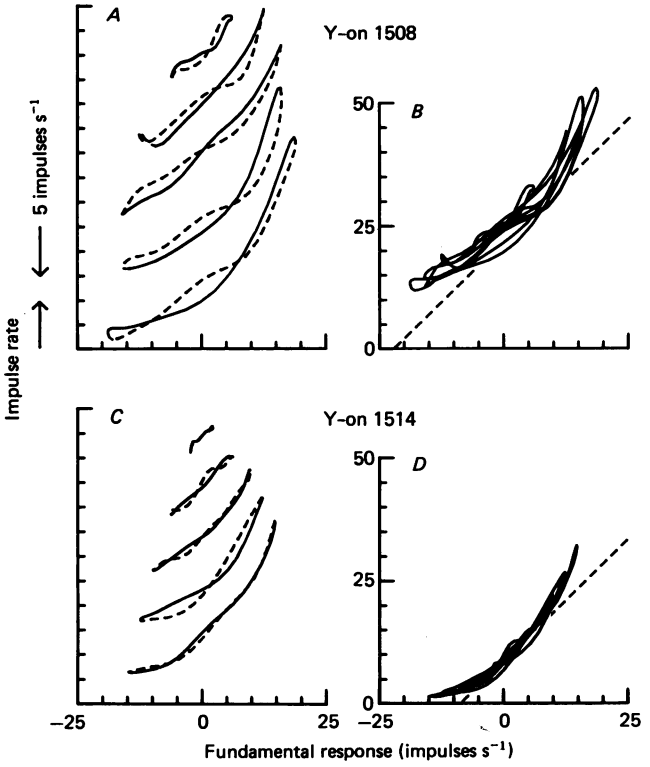

Fig. 3. The static non-linearity in a Y cell's input–output relationship. In *A* and *B*, data from Fig. 1*A* are shown in a different form. Impulse rate at each instant of time during a stimulus cycle is plotted against the instantaneous amplitude of the fundamental response component. Data collected at five stimulus contrasts are shown. They have been displaced vertically in *A* to show the forms of the individual curves (from the top, the contrasts are 0·05, 0·1, 0·15, 0·2 and 0·25), but are superposed in *B*. In *A*, the curve traced out as impulse rate rises to its peak value is shown as a continuous line, and the curve traced out as impulse rate falls is given by the dashed line. The dashed line in *B* shows the input–output relationship expected of a linear mechanism. Results (obtained with the same stimulus contrasts) from a second cell are shown in *C* and *D*.

stimulus to Y cell response includes not only a contrast gain control, but also a static non-linearity with a positively accelerating input–output characteristic. Results for a second cell are shown in Fig. 3*C* and *D*.

The average impulse rate during a stimulus cycle increases with contrast, since the static non-linearity produces greater positive-going excursions than negative-going excursions in the impulse rate. The static non-linearity is therefore a form of rectification. Hochstein & Shapley (1976*b*) suggested that the static non-linearity in Y cells could be either half-wave or full-wave rectification. Fig. 3*B* and *D* show that

it is neither; the input–output characteristic of the rectifier is a smoothly accelerating function for which the vertical deviation from linearity (linear behaviour is represented by the dashed line) is much the same for positive and negative inputs of the same amplitude. Not all units gave as clear a result as that shown in Fig. 3. In particular, the two arms in the plot of impulse rate *versus* fundamental-response amplitude did not always superpose as closely as they do in Fig. 3. There are at least two possible reasons for this behaviour. First, when a bar stimulus is placed over the receptive-field middle it stimulates signal pathways at the middle of the receptive field, and pathways away from the middle. The phase shifts in these pathways differ (see Fig. 4). Secondly, the static non-linearity might be followed by a linear process that shifts response components of different temporal frequencies by differing phases. However, the qualitative effects of rectification, as seen in Fig. 1, were clearly evident in all sixteen units examined.

Linear behaviour

It is our aim in this paper to construct a model for the spatial structure of the Y cell receptive field. To this end it is important to examine not only non-linear behaviour, but linear behaviour as well. Using sinusoidal gratings, Linsenmeier *et al.* (1982) demonstrated that a difference of Gaussians model can be used to fit the linear response component obtained across a range of spatial frequencies when the temporal frequency is 2 Hz. We adopt a similar approach here, with the following differences. First, the spatial profile of the receptive field was determined by placing a narrow bar at a number of locations along a receptive-field diameter, rather than by changing the spatial frequency of a grating. Secondly, the centre and surround components are not constrained to be exactly out of phase with each other in the model we use; it is therefore referred to as a Gaussian centre–surround model, rather than a difference of Gaussians model. Thirdly, rather than using the linear component of a response that also contains non-linear components, a response that is presumed to be entirely linear is analysed. It has already been shown that the Y cell's response approaches linearity as stimulus contrast decreases. The required response measures were therefore obtained from the fundamental Fourier component in the limit as stimulus contrast approaches zero.

An example of the approach is shown in Fig. 2. To measure the cell's responsivity for each placement of the bar, a quadratic function of contrast was fitted by least-squares linear regression to the fundamental amplitudes; the lines in Fig. 2*A* and *B* show the fitted functions. The regression equation used for these fits was $k_1 c + k_2 c^2$ where k_1 and k_2 are constants and c is contrast. The required measure of responsivity is the gradient of the contrast–response function in the limit as contrast approaches zero. This is given by the coefficient, k_1, which has units of impulses s^{-1} contrast-unit^{-1}. The second term, $k_2 c^2$, is included to account for the reduced slope at high contrast. A similar approach is used for the phase of the cell's response. A linear function of contrast, $k_3 + k_4 c$, where k_3 and k_4 are constants, was fitted to the experimental points by least-squares regression. The parameter k_3 is the intercept of the phase curve with the zero-contrast axis; it provides the required measure of response phase in the zero-contrast limit. It will be referred to in the following discussion of linear responses simply as phase. We do not imply that the polynomial

expressions for amplitude and phase are useful as general characterizations for the dependence of the fundamental component on contrast. All that matters here is the fit at low contrasts: the polynomials do a good job in this respect.

Responsivity and phase for two on-centre cells are given as a function of location within the receptive field by the circles in Fig. 4. Location here refers to the mid-point

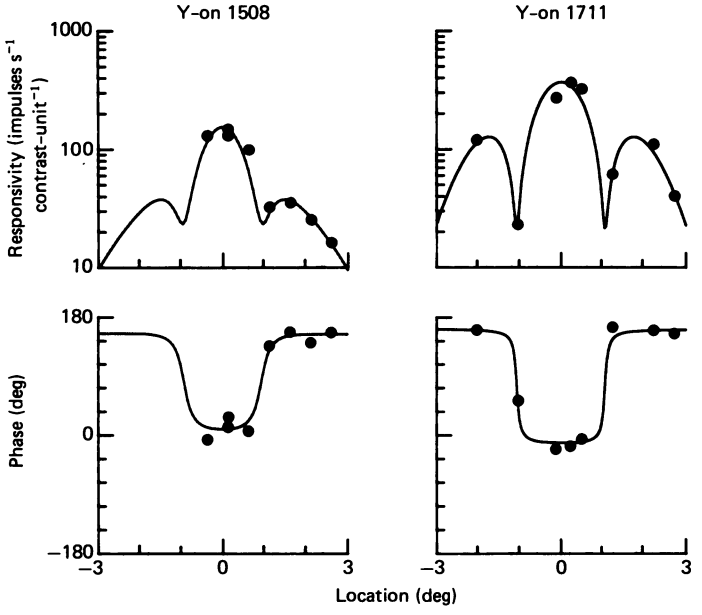

Fig. 4. Receptive-field spatial profiles. A contrast-reversing bar was placed at eight locations across the receptive field; the responsitivities and phases calculated from the fundamental response at each location are shown by the symbols. The continuous curves show the result of fitting a Gaussian centre–surround model to the data from each cell.

of a narrow bar shifted parallel to itself between recordings; the origin of the location axis is placed at the receptive-field middle. For the cell on the left, recordings were taken mostly on one side of the receptive field in order to reduce recording time. The Figure shows that responsivity dies away as the stimulus moves further from the receptive-field middle, but not monotonically. Further, response phase has one value at the receptive-field middle and a quite different value away from it. These observations reflect the well-established result that the Y cell's receptive field is centre–surround organized. Thus, responses to a bar placed at the middle of the receptive field are assumed to be due to a combination of signals from the centre and surround mechanisms, and responses well away from the middle are assumed to be almost entirely due to the surround mechanism. The lines in Fig. 4 were calculated from the best-fitting Gaussian centre–surround model. The form of the model used here and the method by which errors between experimental and model data were minimized are described in the Methods section. The goodness-of-fit was measured by dividing the sum of squared errors by the number of observations and taking the square root. For the data sample of Fig. 4, this root mean squared error was 0·17.

Since the error across all fits in fifteen Y cells was 0·23, the goodness-of-fit in Fig. 4 is slightly better than the average.

Discussion of the centre and surround radius values obtained in fitting the data of Fig. 4 will be postponed until later. Here we describe the values obtained for centre and surround strength and phase. Of particular interest here is the ratio of surround strength to centre strength, since this ratio is one of the major determinants of a cell's behaviour. The mean ratio across fifteen cells was 0·96, indicating that centre and surround strengths were very similar on average. The ratio was quite variable, though, since the standard deviation of the ratio across the same sample was 0·37. This variation between cells can be seen directly in Fig. 5. Responses in this Figure come from two on-centre Y cells, each of which was stimulated with a bar placed close to the receptive-field middle, and also with a bar placed at least one centre radius away from the middle. The Y cell at the top of the Figure had the second highest surround/centre strength ratio (1·23) in the sample. Stimulation away from the middle of this cell's receptive field produced only one response peak (which must therefore have been largely due to the surround mechanism) while stimulation at the middle produced two response peaks, for which the surround-dominated peak was of similar size to the centre-dominated peak. In the lower part of the Figure is another Y cell recorded from the same retina, at about the same eccentricity. This cell has the lowest surround/centre responsivity ratio in the sample (0·32); the surround response is not visible even when the cell is stimulated in the outer receptive field.

In twelve on-centre cells the phase difference between the centre signal and the stimulus averaged −0·5 deg; for three off-centre cells this difference was −172 deg. The closeness of the centre's phase angle to 0 and −180 deg, respectively, is a fortuitous result of choosing 2 Hz as stimulus frequency. The phase angles we have determined for Y cell centres at lower and higher temporal frequencies (unpublished results) are more and less positive, respectively, than those at 2 Hz. Like the ratio of surround strength to centre strength, the difference in phase between the surround and centre signals is an important determinant of the cell's linear behaviour. The surround–centre phase difference in the thirteen cells examined (for two cells, the surround signal was too small to obtain a reliable phase estimate) was always a little less than half a stimulus cycle: mean = 168 deg, standard deviation = 14 deg. Again, the responses of cell 0501 in Fig. 5 give some direct evidence for this result. The peak of the centre-dominated response occurs between zero and one-tenth of the way through a cycle. If the surround signal were exactly out of phase with the centre signal the surround-dominated peak would occur between the fifth- and sixth-tenths; in fact it occurs later. These data on Y cell linear behaviour will be compared with previous results in the Discussion.

Responses to gratings

It has been shown by Hochstein & Shapley (1976*b*) that the frequency-doubled response of a Y cell to a contrast-reversing grating has a higher spatial resolution than that of the linear response component. Any model of the receptive-field spatial structure must obviously take this observation into account. Accordingly, we now describe responses evoked by contrast-reversing gratings, with particular attention to high spatial frequencies. The gratings used were constant in luminance in one

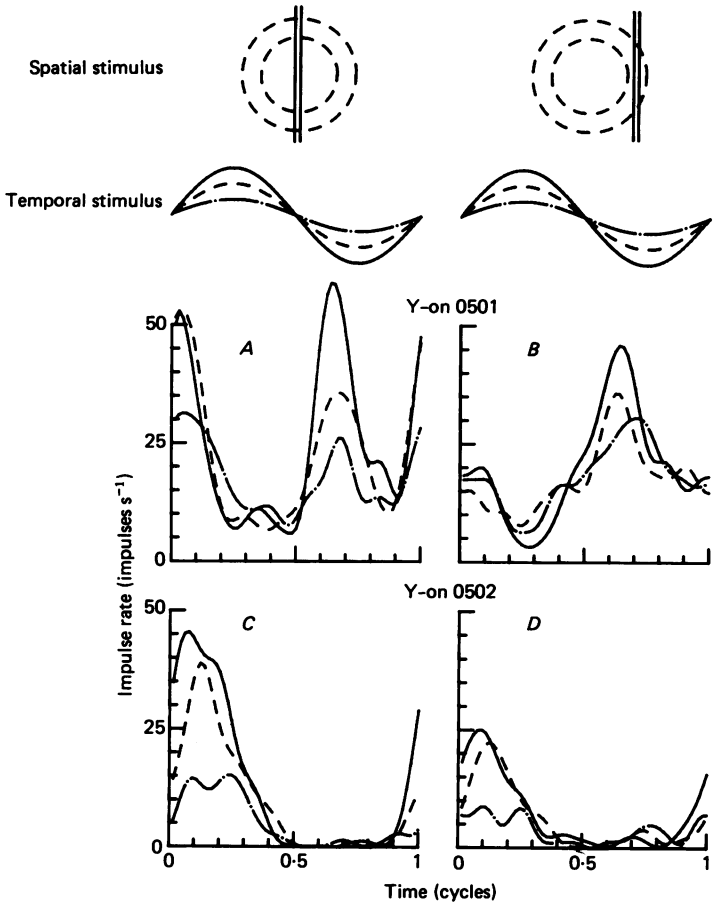

Fig. 5. Demonstration that the strength of the surround mechanism relative to that of the centre varies markedly from cell to cell. A contrast-reversing bar was placed at the middle and outer receptive field of two cells. The mid-points of the bars were placed 2·2 and 0·5 deg from the receptive-field middle in *B* and *D*, respectively. The minimum contrast presented was 0·2 for each set of axes; stimuli were presented at multiples (1, 2 and 3) of these minimum contrasts. The data collection period was 7 s for each contrast.

spatial dimension and modulated sinusoidally in the perpendicular spatial dimension. Gratings were stationary, and luminance at each point was modulated as a sinusoidal function of time with a temporal frequency of 2 Hz.

Fig. 6 shows the responses of two on-centre cells and one off-centre cell (the same cells as in Fig. 1) to gratings of two spatial frequencies placed in even symmetry about the receptive-field middle. Impulse rate as a function of time during the stimulus cycle is shown for four contrasts at each spatial frequency. These responses display some of the properties already noted in the response to contrast-reversing bars. First, they are rectified; positive-going impulse rate excursions are greater than negative-going ones. Secondly, response peaks occur earlier in the cycle when contrast is increased. Finally, the off-centre cell behaves similarly to the on-centre cells except that its

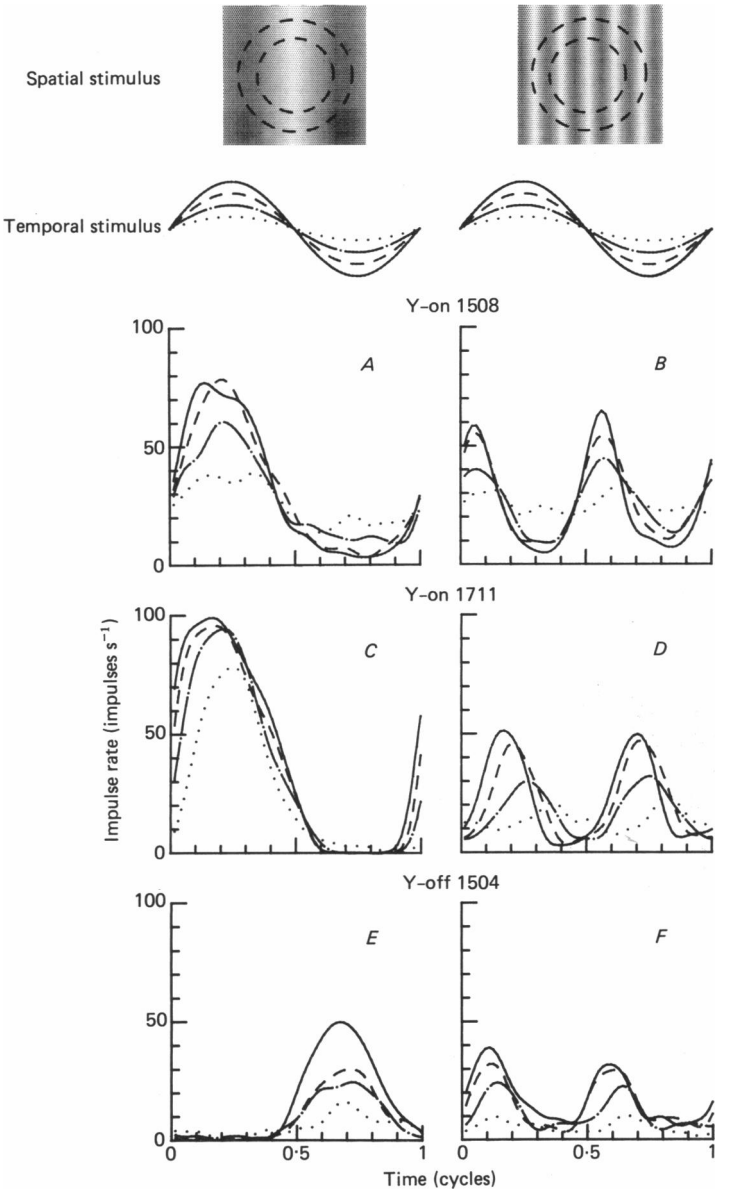

Fig. 6. Impulse rate profiles for a grating stimulus. Luminance varied sinusoidally across the grating and mean luminance was 420 cd m^{-2}. Spatial frequencies of 0·34 and 1·24 cycles deg^{-1} were used, as shown at the top of the Figure. The radii of the inner and outer dashed circles roughly approximate the radii of the centre and surround, respectively, of a Y cell. Gratings were placed in even symmetry about the receptive fields. Luminance varied as a sinusoidal function of time at 2 Hz, as shown by the wave forms below the gratings. Four contrasts (shown by dashed lines of different types) were presented at each spatial frequency for each of the three cells represented. The contrasts were integral multiples (1, 2, 3 and 4) of the following minimum contrasts: *A*, 0·025; *B*, 0·1; *C*, 0·025; *D*, 0·1; *E*, 0·033; and *F*, 0·1. The data collection period was 10 s for each contrast.

responses are shifted by about half a cycle. It is also clear that responses are dominated by the fundamental Fourier component at low spatial frequencies, and are frequency doubled at high. In what follows, we concentrate on the second-harmonic component of the response, and its dependence on spatial frequency; this analysis will provide a measure of the spatial summation area of the mechanism responsible for frequency doubling.

In Fig. 7 the amplitude of the second Fourier harmonic in eight Y cells is plotted against stimulus contrast for the response to a contrast-reversing grating; the spatial frequency of the grating is around 2 cycles deg^{-1} in all cases. The slopes of these curves

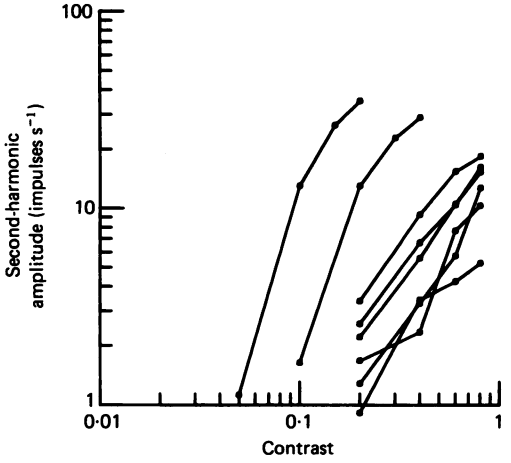

Fig. 7. Effect of contrast on the second-harmonic response component. A contrast-reversing grating with a spatial frequency close to 2 cycles deg^{-1} was used to stimulate eight Y cells. The grating was placed in even symmetry about the middle of the receptive field (at the spatial frequency used, the placement did not affect the response). Lines connect the points recorded from an individual cell.

are between 1·2 and 3·5 at low response amplitudes, with most of them equal to 1·4 or 1·5; slopes are reduced at higher amplitudes. The regression function used to fit these data was $k_1 c^2 + K_2 c^3$, where k_1 and k_2 are constants and c is contrast. The second-power term is included to provide an approximate match with low-amplitude points (since it implies a slope of 2), and the third-power term to account for the reduced slope at higher amplitudes. As contrast approaches zero, the regression function reduces to the term involving the square of contrast, and the dependence of the second harmonic on contrast can be characterized by the coefficient, k_1, which has units of impulses s^{-1} contrast-unit^{-2}. As with the analysis of linear responses, use of the low-contrast coefficient means that the measurement is independent of the contrast gain control and the effects of clipping at 0 impulses s^{-1}. Fig. 8*A* gives the amplitude of the second harmonic per squared contrast-unit, k_1, as a function of spatial frequency for a total of seven Y cells. The frequency-doubled response of a Y cell decreases rapidly with increasing spatial frequencies in the region of 1–4 cycles deg^{-1}. It needs to be stressed that the forms (though not the vertical location) of the curves in Fig. 8 are largely independent of the regression function used to fit contrast–

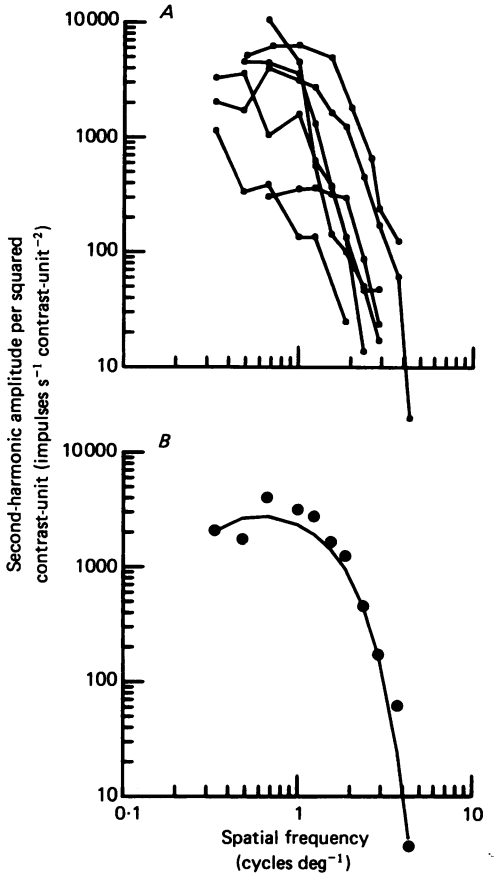

Fig. 8. Spatial tuning of the second-harmonic response component. The growth of second-harmonic amplitude with contrast was fitted with a function proportional to the square of contrast at low contrast. This Figure plots the coefficient of squared contrast in the fitted function against the spatial frequency of the grating used. Gratings were placed in odd symmetry about the receptive field at low spatial frequencies, but were placed in either odd or even symmetry at higher spatial frequencies, where the response did not vary with the spatial phase of the stimulus. *A*, lines join the experimentally determined points from each cell, with seven cells represented. *B*, circles show the experimental points from one cell (*Y*-on 1712). The line in *B* shows the result of fitting the pooled subunits model by least-squares non-linear regression.

response curves. The other functions tested were $k_1 c + k_2 c^2$ (which yields a contrast–response coefficient with units of impulses s^{-1} contrast-unit^{-1}) and $k_1 c^2/(1 + k_2 c^2)$.

The range of spatial frequencies in which the frequency-doubled response decreases rapidly can be conveniently characterized with a single number by fitting a Gaussian function of spatial frequency, $k \exp[-(\pi r_{fd} u)^2]$, to the curves in Fig. 8*A*. In this formulation k is a constant, u is spatial frequency, and r_{fd} is the spatial parameter used to characterize the point of rapid decrease; r_{fd} will be termed the *frequency-doubling radius*. Fig. 8*B* shows data from one unit (circles) along with the function fitted to it (continuous line). The actual function fitted was the response of the

complete receptive-field model, described by eqn. (16) in the Appendix. This function approaches $k \exp[-(\pi r_{fd} u)^2]$ as spatial frequency increases. Fitting was performed by minimizing the sum of squared errors; the error at each spatial frequency was computed by finding the difference between the contrast–response coefficient of the cell's second-harmonic component and that of the model's second harmonic, and dividing that difference by the cell's coefficient.

Spatial parameters of the Y cell receptive field

Estimates of the frequency-doubling radius, r_{fd}, obtained by fitting a Gaussian function of spatial frequency to the second-harmonic response are shown by the circles in Fig. 9*A*. Each point gives the estimate for one cell; seven Y cells in total are represented. Points are plotted against receptive-field eccentricity, as estimated by the procedure described in the Methods section. The results are represented this way because of the finding that spatial scales become larger as distance from the area centralis increases (e.g. Wiesel, 1960; Enroth-Cugell & Robson, 1966; Peichl & Wässle, 1979). However, our sample is probably too small to be able to say whether the spatial summation area of the frequency-doubled response increases with eccentricity. The dashed line in Fig. 9, taken from the work of Linsenmeier *et al.* (1982), gives the regression line for the radius of the centre mechanism across a large population of X cells. So & Shapley (1979) showed that linear responses of X cells in the lateral geniculate nucleus have approximately the same spatial resolution as frequency-doubled responses of lateral geniculate Y cells. It is apparent from Fig. 9*A* that the same is true of X and Y cells in the retina.

Above the dashed line are plotted two more sets of points, both of which were obtained earlier in the paper from the analysis of Y cell linear responses. They are the centre radii and the surround radii obtained across a larger sample of cells than those represented by the frequency-doubling results. Since the centre and surround radii were obtained by fitting a Gaussian centre–surround model to Y cell linear responses, they give an estimate of the spatial resolution of the linear response. When the resolution of the X cell (linear) response is compared with that of the Y cell linear response, the finding (e.g. Cleland, Harding & Tulunay-Keesey, 1979) that X cells operate on a spatial scale finer than that of Y cells is borne out. Again comparing results with those of Linsenmeier *et al.* (1982), our Y cell centre radii are slightly larger than theirs; the reason for this discrepancy is not clear. An explanation of Fig. 9*B* must wait until the receptive-field model has been described.

A model for the spatial structure of the receptive field

We now have the observations required to test a new receptive-field model. Hochstein & Shapley (1976*b*) showed that the Y cell receptive field can be described as containing a number of parallel channels called *subunits*. A subunit is defined by two essential properties: a small spatial spread compared with the complete receptive field, and a rectifying input–output function. The receptive-field model to be used here is shown in Fig. 10. The model contains a number of localized, rectifying channels which, by analogy with Hochstein & Shapley's terminology, will be called subunits. Each subunit pathway has a centre–surround spatial organization followed by a rectification element. Subunit signals across the receptive field are weighted and

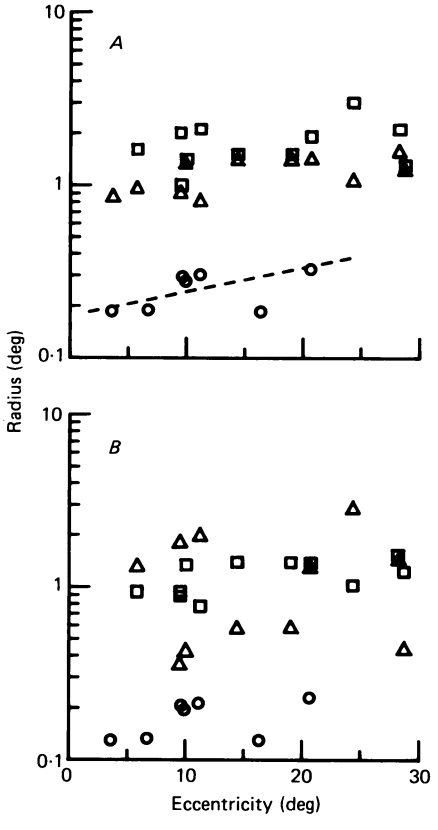

Fig. 9. Spatial scale of receptive-field mechanisms. *A*, the radius of the Gaussian mechanism that best fits the decrease in the frequency-doubled response with increasing spatial frequency (as shown in Fig. 8) is plotted by ○. Centre and surround radii, determined by fitting a Gaussian centre–surround model to linear responses (see Fig. 4) are shown by △ and □, respectively. A total of sixteen Y cells is represented, but for some cells, only one or two of the radii were determined. The dashed line shows the regression line determined by Linsenmeier *et al.* (1982) for the centre radius in a large population of X cells. *B*, radius values in the pooled subunits model, as determined by substituting the radii in *A* into eqns. (5) and (10). Subunit centre and subunit surround radii are shown by ○ and △ respectively. Pool radii are shown by □.

summed by a *pool* mechanism, and the pool is followed by a contrast gain control element. The model performs spatial processing on the stimulus through the subunit centre–surround and pool elements, and it performs temporal processing through the subunit centre–surround and contrast gain control elements. For ease of reference, and in order to distinguish it from other possible models, the model of Fig. 10 will be referred to as the *pooled subunits model.*

Four assumptions are made in the model which are not explicitly shown in the Figure. The model is assumed to be unaffected by the mean level of the stimulus. All data used in this study were collected at a single adaptation level and no attempt has been made to build an adaptation mechanism into the model. Secondly, neighbouring subunits are assumed to overlap, and the retinal distance between their

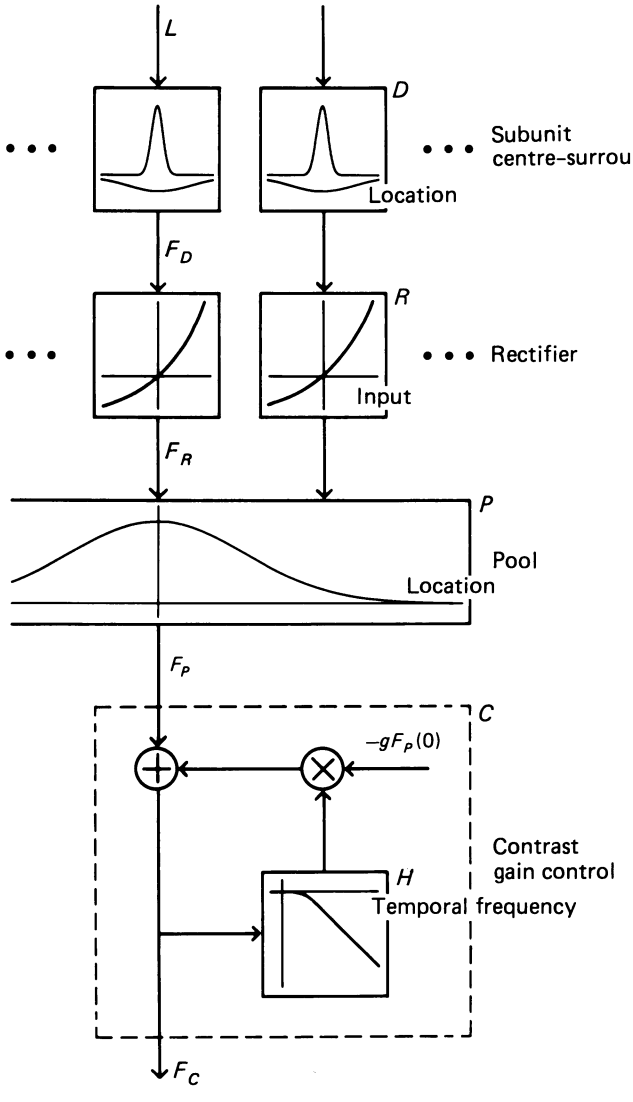

Fig. 10. Pooled subunits model. L represents the fundamental component of the stimulus. F represents the Fourier components of an element's output signal; F_P, for example, represents the pool's output, and $F_P(0)$ the d.c. component of that output. The remaining upper case letters represent the frequency responses of individual elements. The input–output relationships for all elements are given below. For some, this relationship is not easily expressed as a frequency response and is instead given in terms of the output signal as a function of time, $f(t)$. Thus, for instance, the output of element R is given as $f_R(t)$.

$$D(x, y, x_{\text{sub}}, y_{\text{sub}}) = \pi^{-1} r_{\text{sc}}^{-2} S_{\text{c}} \exp[-[(x-x_{\text{sub}})^2+(y-y_{\text{sub}})^2] r_{\text{sc}}^{-2}] + \pi^{-1} r_{\text{ss}}^{-2} S_{\text{s}} \exp[-[(x-x_{\text{sub}})^2+(y-y_{\text{sub}})^2] r_{\text{ss}}^{-2}],$$

$$f_R(t) = f_D(t) + q f_D^2(t), \quad P(x, y) = \pi^{-1} r_{\text{p}}^{-2} \exp[-(x^2+y^2) r_{\text{p}}^{-2}],$$

$$H(w) = (1+i2\pi\tau w)^{-1}, \quad C(w) = [1+gF_P(0)H(w)]^{-1}, \quad f_M(t) = m + f_C(t),$$

where: f_M = model output; g = coefficient of gain-changing signal in contrast gain

mid-points is assumed to be infinitesimally small in order to simplify the model and its mathematical analysis. This assumption is justified so long as receptive-field spatial profiles do not show any small-scale bumpiness. Thirdly, while the Figure implies that the output from a subunit centre–surround combination is obtained by subtracting the subunit surround signal from the subunit centre signal, no such requirement is made in the model; the phase difference between the two components can differ from 180 deg, if necessary. The final assumption is that the (continuously variable) output of the contrast gain control is fed to an integrate-and-fire mechanism which yields an impulse train with a non-zero resting level (the maintained discharge). When the input to the integrate-and-fire mechanism is negative, no impulses are generated. We now discuss the basis for the model by describing its linear and non-linear behaviour, and show how these relate to the experimental findings.

Linear behaviour of the model

Given the result that the linear component of the Y cell's response to different spatial stimuli can be described by a Gaussian centre–surround model, it needs to be shown that the pooled subunits model reduces to a Gaussian centre–surround form when only its linear component is considered. When stimulus contrast is low enough, signals in the subunit pathways of the pooled subunits model fall on the approximately linear portion of each rectifier's input–output function. Also at low contrast, the time-invariant d.c. component in the pool's output is small and the feed-back signal in the contrast gain control (which is controlled by the pool's d.c. output) approaches zero. In the limit as contrast approaches zero, therefore, the rectifiers and contrast gain control can be neglected; the model is then equivalent to a sum of subunit centre–surround spatial profiles, where each profile is weighted by the gain of the pool mechanism at the location of the subunit in question. This pooling produces a centre mechanism that is wider than both subunit centre and pool, and a surround mechanism wider than subunit surround and pool. It turns out that when the subunit centre, subunit surround and pool mechanisms have Gaussian spatial profiles, the pooled centre and surround mechanisms are also Gaussian. The linear part of the model is thus Gaussian centre–surround in its spatial form.

In the terminology of linear systems analysis, the linear part of the pooled subunits model has a spatial impulse response equal to the space convolution of the subunit centre–surround and pool impulse responses. In the spatial frequency domain, this means that the model's frequency response is the product of the subunit centre–surround and pool frequency responses. Denote spatial frequency by u, the frequency response of the subunit centre–surround combination by $D(u)$ and the pool frequency response by $P(u)$. Fourier transformation of the spatial impulse responses defined in the legend of Fig. 10 gives

$$D(u) = S_c \exp[-(\pi r_{sc} u)^2] + S_s \exp[-(\pi r_{ss} u)^2], \quad (2)$$

$$P(u) = \exp[-(\pi r_p u)^2]. \quad (3)$$

---

control; $i = \sqrt{-1}$; m = maintained discharge (impulse rate for a steady, uniform stimulus); q = coefficient of rectifier non-linear component; r_{sc}, r_{ss}, r_p = radii of subunit centre, subunit surround and pool; S_c, S_s = vectors with strength and phase of subunit centre, and subunit surround; t = time; τ = time constant of contrast gain control; w = temporal frequency; (x, y) = location on retina relative to receptive field middle; (x_{sub}, y_{sub}) = location of middle of subunit.

Thus, the model's frequency response is

$$D(u)P(u) = S_c \exp[-(\pi r_c u)^2] + S_s \exp[-(\pi r_s u)^2], \tag{4}$$

where the pooled centre and pooled surround radii are given by

$$r_c^2 = r_{sc}^2 + r_p^2; \quad r_s^2 = r_{ss}^2 + r_p^2. \tag{5}$$

This result shows that, like the spatial organization of the subunit, the frequency response of the complete model is Gaussian centre–surround in form; the model's centre has a radius of $r_c = \sqrt{(r_{sc}^2 + r_p^2)}$ and the model surround's radius is $r_s = \sqrt{(r_{ss}^2 + r_p^2)}$.

In the following, the pooled centre and pooled surround will be referred to simply as the centre and surround.

Non-linear behaviour of the model

The features that make the pooled subunits model non-linear are the rectifiers and contrast gain control; the rectifiers are considered first. Suppose that the input to a rectifier is $f(t)$, a function of time, and that its output is $g(t)$. The form used for the rectifier is

$$g(t) = f(t) + qf^2(t), \tag{6}$$

where q is a constant. There are three major reasons for this choice.

(1) Apart from the maintained discharge, the input–output relationship for the static non-linearity shown in Fig. 3*B* and *D* is adequately modelled by eqn. (6). The dashed line represents the term $f(t)$ in the equation. Subtraction of values on the dashed line from the recorded impulse rate give a remainder corresponding to the term $qf^2(t)$. The approximately parabolic form of the computed differences indicates that the power of two in $qf^2(t)$ is justified.

(2) The fundamental Fourier component and second harmonic are responsible for almost all the time-varying a.c. power in the responses recorded in this study. As an example of this, the responses of cell 1508 in Figs. 1 and 6 were analysed; this cell was chosen since its responses are not clipped at 0 impulses s^{-1}. The data recorded at the largest contrast on each set of axes were used since they are the most non-linear. The summed power in the fundamental and second-harmonic components contributed 92 % of the total a.c. response power. The number of harmonics generated by the model can be determined directly from eqn. (6). The subunit pathway preceding a rectifier is linear, so that the input to the rectifier can be put in the form $f(t) = kc \cos(2\pi wt + p)$ where k is a constant, c is contrast, w is temporal frequency and p is phase. Then, by standard trigonometry,

$$\begin{aligned} g(t) &= f(t) + qf^2(t) \\ &= kc \cos(2\pi wt + p) + \tfrac{1}{2}qk^2c^2[1 + \cos 2(2\pi wt + p)] \\ &= \tfrac{1}{2}qk^2c^2 + kc \cos(2\pi wt + p) + \tfrac{1}{2}qk^2c^2 \cos 2(2\pi wt + p). \end{aligned} \tag{7}$$

The first term is the d.c. response of the rectifier since it does not vary in time, the second is its fundamental Fourier component, and the third, which has a temporal frequency twice that of the stimulus, is the second harmonic. The model, then, predicts that all the response power is in the d.c. response, fundamental and second harmonic. Adding a term of power three or higher to the input–output relationship for the rectifier would add third or higher harmonic terms to eqn. (7). The experimental

results show that if there are terms of higher order than two in the input–output relationship for the static non-linearity, their coefficients must be small compared to the other coefficients.

(3) Eqn. (7) requires that a log–log plot of the second harmonic's amplitude *versus* contrast yield a slope of two. The slopes obtained from the eight Y cells represented in Fig. 7 were mostly 1·4 or 1·5. A power of two is used in the model since an integral value results in a simpler analysis, and there is reason to believe that a more detailed experiment would yield a higher power than that determined here (see the Discussion).

The other source of non-linearity in the model is the contrast gain control. The form used for this element is taken in part from the modelling work of Shapley & Victor (1981); it is assumed to be a feed-back loop in which there is a temporal low-pass filter in the feed-back arm. The gain of the feed-back path is here assumed proportional to a low-pass filtered version (in practice, the d.c. component) of the signal leaving the pool mechanism; the feed-back gain therefore increases with contrast. This choice for the gain-changing signal is justified in the Discussion. Increasing contrast has two effects in the resulting model: a relatively larger feed-back signal is subtracted from the input to the contrast gain control and the gain of the system therefore falls; since the low-pass filter delays the feed-back signal relative to the input, subtraction of the feed-back signal advances the phase of the output signal.

The model's spatial parameters

The results in Fig. 9*A* can be rearranged to obtain direct estimates of radii in the pooled subunits model. Consider first the subunit centre radius, r_{sc}. This quantity determines the range of spatial frequencies in which the frequency-doubled response to a contrast-reversing grating decreases rapidly, since these spatial frequencies are higher than the spatial resolutions of the subunit surround and pool mechanisms. In this range, the model therefore approaches a limit in which it looks like a single subunit centre mechanism followed by a rectifier. The second harmonic then has amplitude proportional to

$$(\exp[-(\pi r_{sc}\, u)^2])^2 = \exp[-2(\pi r_{sc}\, u)^2]. \tag{8}$$

Equating this to the function already used to fit the curves in Fig. 8 yields

$$\exp[-2(\pi r_{sc}\, u)^2] = \exp[-(\pi r_{fd}\, u)^2], \tag{9}$$

and

$$2r_{sc}^2 = r_{fd}^2. \tag{10}$$

Thus the subunit centre radius of the model can be obtained by dividing the experimentally determined frequency-doubling radius by $\sqrt{2}$.

Eqns. (5) and (10) together provide the transformations required to derive the model radii in Fig. 9*B*. For each Y cell, the three known values, frequency-doubling radius, r_{fd}, centre radius, r_c, and surround radius, r_s, were used to determine the three unknowns, subunit centre, subunit surround, and pool radii, r_{sc}, r_{ss}, and r_p, respectively. For nine cells, grating stimuli were not presented and no direct estimate of the frequency-doubling radius obtained. For these cells, the estimate used for the frequency-doubling radius is from a regression line through the frequency-doubling results in Fig. 9*A*. The estimates of subunit surround radius in the lower graph are

scattered, but subunit centre and pool radii have quite consistent values across the sample.

Reconstruction of the Y cell response

The ability of the pooled subunits model to account for either Y cell linear or non-linear behaviour has been discussed. It is of obvious interest to see how well the model can predict responses containing both linear *and* non-linear components. A difficult test for the model is a prediction of impulse rate *versus* time for a specific spatial configuration; this test requires the prediction of not only a single Fourier component of the response, but of all components and their correct combination. The analysis in the Appendix provides equations for the response of the model to a contrast-reversing grating with variable spatial frequency and phase, and the response to a contrast-reversing bar at an arbitrary location in the receptive field. Those equations are used in the following reconstruction (the integration in eqn. (21) was performed numerically).

Model parameters were obtained from various sources. The radii are those depicted in Fig. 9*B*, subunit centre and surround strengths and phases were obtained by fitting the Gaussian centre–surround model to linear responses, as previously described, and the maintained discharge was estimated from the impulse rate recorded when the stimulus was modulated neither in space nor time. The time constant (τ) in the contrast gain control was set so that τw took the arbitrary value of 1 radian; temporal frequency was not varied and there was therefore little basis for optimizing its value. The two remaining parameters, q and g (coefficient of the rectifier's non-linear component, and coefficient for the gain-changing signal in the contrast gain control, respectively) were adjusted to obtain the best match between cell and model responses, as judged by eye. The uppermost graphs in Figs. 11 and 12 were generated with a single set of model parameters, that estimated for cell 1508, and are to be compared with the responses of cell 1508 in Figs. 1 and 6. Similarly, there are comparisons between experimental and model responses for two other cells. It should be realized that the model parameters have not been optimized to obtain the best fit of the model to the displayed experimental results; rather, the parameters have come from a variety of sources.

In Fig. 11, the model qualitatively accounts for: the way in which impulse rate as a function of time changes from a sinusoidal function to a rectified function as contrast increases; the change in response phase when the bar is shifted from the receptive-field middle to a location in the outer field; some of the phase advance that occurs with increasing contrast, and the small response increments at high response amplitudes. Similarly, in Fig. 12, the model accounts qualitatively for the way in which the impulse rate profile changes with increasing contrast, and it reproduces the frequency-doubled response that occurs at the higher spatial frequency. Finally, there is an important property of the Y cell receptive field that the model must satisfy if it is to be considered realistic; the property is not illustrated in Figs. 11 or 12. At high spatial frequencies, the Y cell's frequency-doubled response is independent of spatial phase (Hochstein & Shapley, 1976*a*). The analysis in the Appendix shows that the model reproduces this behaviour. Response features for which the model cannot account are taken up in the Discussion.

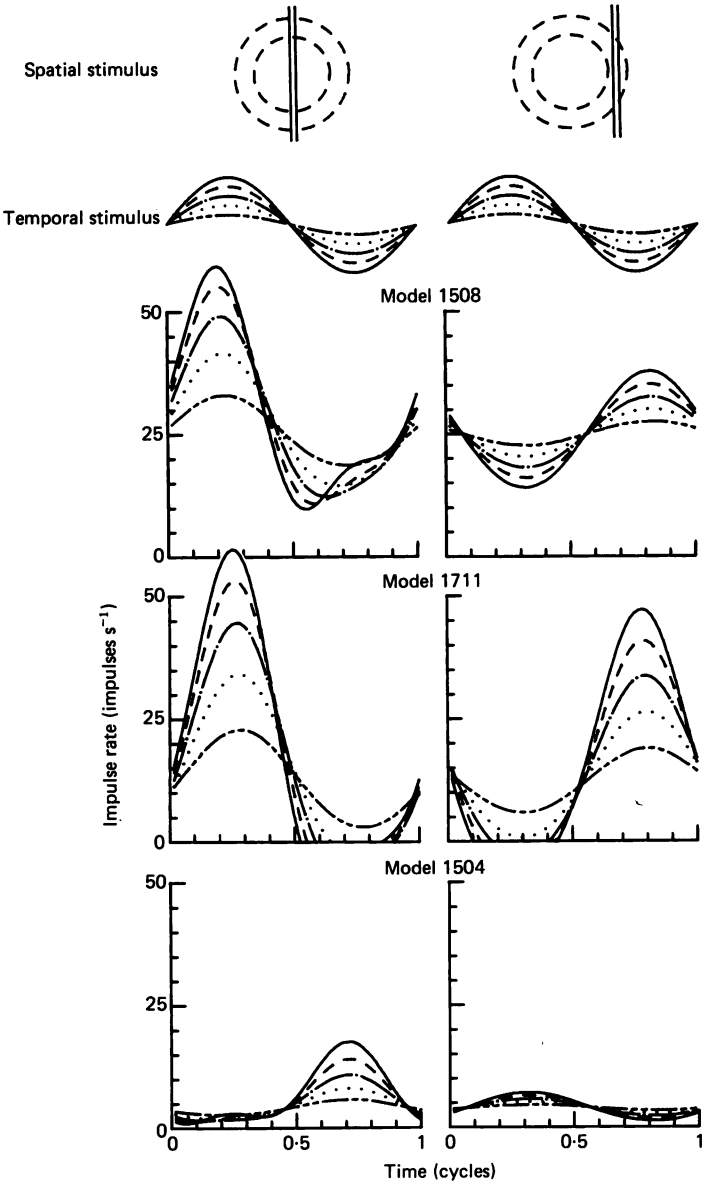

Fig. 11. Reconstruction of the Y cell response to a contrast-reversing bar. The Figure is the same as Fig. 1 except that impulse rates predicted by the pooled subunits models for cells 1508, 1711 and 1504 have been substituted for experimentally determined impulse rates in those cells. The parameter values used were: cell 1508: $|S_c| = 1170$ impulses s^{-1} contrast-unit^{-1}; phase $(S_c) = -2$ deg; $r_{sc} = 0{\cdot}21$ deg; $|S_s| = 1020$ impulses s^{-1} contrast-unit^{-1}; phase $(S_s) = 155$ deg; $r_{ss} = 2{\cdot}0$ deg; $q = 0{\cdot}0040$ s impulse^{-1}, $r_p = 0{\cdot}77$ deg; $\tau = 80$ ms; $g = 0{\cdot}11$; $m = 25$ impulses s^{-1}; cell 1711: 78800, −18, 0·20, 78300, 162, 0·42, $8{\cdot}0 \times 10^{-6}$, 1·3, 80, 0·080, 12; cell 1504: 212, −171, 0·13, 123, −23, 2·9, 0·020, 0·84, 80, 0·030, 4·0.

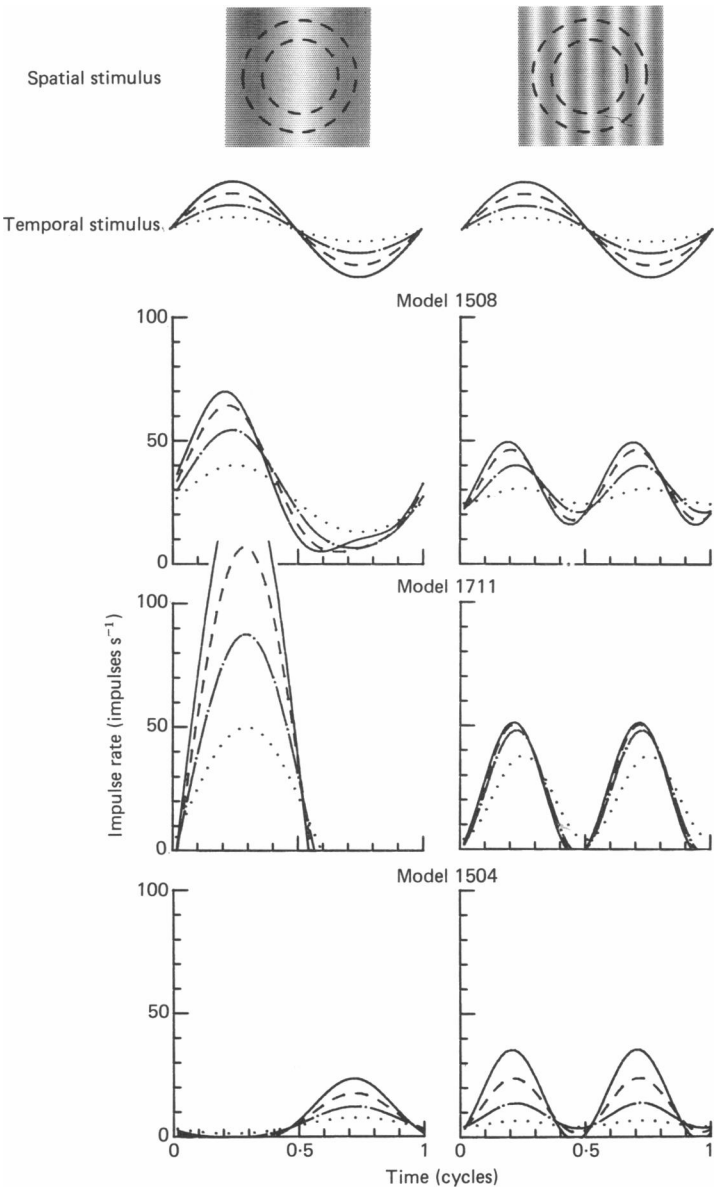

Fig. 12. Reconstruction of the Y cell response to a contrast-reversing grating. The stimulus conditions are the same as those in Fig. 6. The impulse rates were generated by the same three sets of model parameters as in Fig. 11.

DISCUSSION

We first compare our experimental results with previous work. Then the structure and adequacy of the pooled subunits model are discussed in some detail.

Linear responses

The contrast gain control has at least two effects on the responses of both X and Y cells in the cat retina; response amplitude grows less than proportionally with stimulus amplitude at low temporal frequencies of stimulation, and response phase is advanced (Shapley & Victor, 1978). Because of these effects, the parameters describing Y cell linear behaviour were determined in the present study at the limit as contrast approached zero, where the effect of the contrast gain control is presumed to be absent. Previous studies of X and Y cell linear behaviour (Derrington & Lennie, 1982; Linsenmeier *et al.* 1982; Enroth-Cugell *et al.* 1983) used a different approach. For each spatial configuration of the stimulus, contrast was adjusted to obtain a constant response criterion, typically a fundamental Fourier component of about 10 impulses s^{-1}. Because the contrast gain control was active, it can be expected that the contrast sensitivities and responsivities determined in those previous studies would be lower and the responses more advanced than would be the case for a determination at the zero-contrast limit.

Since the contrast gain control seems to act in similar fashion on both centre and surround mechanisms (see the centre- and surround-dominated responses in Fig. 1), comparisons between the centre and surround strengths found here and in previous studies will be facilitated by comparing the surround strength/centre strength ratio, rather than the absolute strengths. In our limited sample of cells, we find that for stimuli temporally modulated at 2 Hz, centre and surround strengths are about equal on average. This is a conclusion quite different from that of Derrington & Lennie (1982), who determined a surround/centre strength ratio of 0·56 (average across eight Y cells stimulated at 2·6 Hz), and Linsenmeier *et al.* (1982) who found a strength ratio of 0·73 in a sample of eighty-nine cells that included both X and Y cells. The discrepancy is probably at least partly due to the fact that response phase is taken into account in our estimate, whereas response phase was not measured in the previous determinations. In the present sample, the average difference between the phase angles of the surround and centre signals is 168 deg. When a cell with equal centre and surround strength and a surround–centre phase difference of 168 deg is stimulated with a spatially uniform stimulus, it will produce a fundamental amplitude that is 0·21 times the amplitude of the centre signal. Interpreting this observation in terms of a model with a surround–centre phase difference of 180 deg, as used by Derrington & Lennie and Linsenmeier *et al.* would lead to a surround/centre strength ratio of $1-0{\cdot}21 = 0{\cdot}79$, which is in the direction of their determinations.

The model used by Enroth-Cugell *et al.* (1983) to describe spatiotemporal interactions in cat retinal X cells, the Gaussian centre–surround model, assumes that the signal in the surround pathway is not only inverted relative to that in the centre pathway but is also delayed. Their data were best fitted when the surround signal was delayed relative to the centre signal by intervals from 1·2 to 7·7 ms. The average difference between the surround and centre phases found here for Y cells stimulated at 2 Hz, 168 deg, translates into a time delay of $1000 \times (180-168)/(360 \times 2) = 17$ ms. The disparity between these two results indicates that the dynamic behaviour of X and Y cells differs markedly, at least at photopic adaptation levels and frequencies around 2 Hz.

Non-linear responses

Fig. 1 confirms that there is a rectifier present in the Y cell signal pathway; we chose to represent the non-linear part of the rectifier with a square law device, $g = f^2$. Victor & Shapley (1979) suggested instead that the most appropriate form for the rectifier was a power of the input magnitude, $g = |f|^p$, where the power, p, is close to one. Since both functions are of the form $|f|^p$, the question reduces to the correct value for p: is the power closer to one or two? Probably the best data with which to settle this issue are recordings of the amplitude of the Fourier second harmonic as a function of stimulus contrast. When this function is plotted on log–log axes, its gradient as contrast approaches zero is equal to the power p. Hochstein & Shapley (1976*b*) found that a power of one suited their data, and Victor & Shapley (1979) used a power of about 0·9. We find, as in Fig. 8, that the power is usually 1·4 or 1·5. There are two confounding factors in the measurement of this quantity. At high contrast levels, the contrast gain control comes into action, and the gradient of the contrast–response function falls. At low contrast levels, data collection periods have to be long to avoid contamination of the data with noise. It is possible that we found a higher power for the contrast–response function than did the previous studies because the contrast gain control was less influential in our determination. It is also possible that stimulus–response powers higher than ours could have been demonstrated if longer data collection periods and lower contrasts had been used.

Previous models

In the model for Y cell receptive-field structure described by Hochstein & Shapley (1976*b*) and Victor & Shapley (1979), linear and non-linear signals proceed along independent sets of pathways. In the pooled subunits model, linear and non-linear responses are assumed to derive from the same set of pathways. Are these two views reconcilable? Ignore the effect of the contrast gain control for the moment, since the location of the rectifier is the main question here. Our model can be formally separated into linear and non-linear pathways: since the rectifier is assigned the form $g = f + qf^2$, where f and g are input and output, respectively, the model's output can be expressed as the sum of a linear component, deriving from the f term, and non-linear component, deriving from the qf^2 term. This does not help in interpreting physical mechanisms in the retina, however, since the two components are assumed to undergo exactly the same processing except within the rectifier.

The main piece of evidence supporting the idea that linear and non-linear pathways are independent in the Y cell receptive field comes from the work of Frishman & Linsenmeier (1982). They showed that when picrotoxin is applied systemically, Y cell second-harmonic responses to a contrast-reversing grating were reduced while the fundamental response component due to a drifting grating was unaffected. If the model we have proposed is to be consistent with this result, the non-linear component of the rectifier would have to be reduced by picrotoxin without affecting the linear component. That is, the rectifier would have to be straightened out by picrotoxin.

Some of the features of the pooled subunits model are present in a receptive-field model suggested by Cleland (1983). In Cleland's model the linear centre and surround mechanisms are both assumed to be composed of a weighted array of spatially smaller

mechanisms (*subunits*); the model therefore requires that linear and non-linear responses be due to the same set of mechanisms. Cleland did not, however, specify the model in sufficient detail to test its prediction against experimental data.

Model organization

Given the properties that a model for the Y cell receptive field has to incorporate, centre–surround behaviour, rectification, pooling, and contrast gain control, the elements giving rise to these properties can be arranged in more than one way. The following observations limit the possible arrangements.

(1) Centre–surround antagonism must precede rectification, for two reasons. First, depending on the centre type of a cell, there must be a sign inversion in the surround pathway that is not present in the centre pathway, or an inversion in the centre pathway that is not present in the surround pathway. If this extra sign inversion followed rectification then it should be possible to find responses in which negative excursions of the impulse rate exceed positive excursions: these were not observed. Secondly, suppose that centre and surround signals pass through rectifiers before being combined. Then a spatially uniform contrast-reversing stimulus will yield large fundamental and second-harmonic signals in both pathways, of which only the fundamental component will be reduced substantially by centre–surround antagonism. Again, this is not observed. Responses to a low spatial frequency grating, as in Fig. 6, are dominated by the fundamental component.

(2) As Hochstein & Shapley (1976*b*) have pointed out, pooling must occur after rectification in order that frequency-doubled responses have a higher spatial resolution than linear responses.

(3) The contrast gain control need not be limited to its position after the rectifier. Indeed, if gain controls occur at several levels in the retina (see Shapley & Enroth-Cugell, 1984), then it is possible that the contrast gain control be distributed across a number of locations in the signal pathway. All that is required here is that some contrast gain control be present after the rectifier; the responses to the finer grating in Fig. 12 show why. Suppose that there is no contrast gain control following rectification. Since the linear component of the response to a fine grating is negligibly small, only the components resulting from the squaring operation of the rectifier need be considered. And since squaring is involved, the impulse rate must always be greater than the maintained discharge. This prediction contradicts the experimental observation. Suppose there is contrast gain control following the rectifier. Then the squaring operation of the rectifier produces a d.c. response and second harmonic, and because of the high-pass frequency response assumed for the contrast gain control, the d.c. response is attenuated more than the second harmonic. Impulse rate in the model can therefore fall below the level of the maintained discharge, as required.

(4) Gain along the feed-back pathway in the contrast gain control is assumed to increase with contrast, and to be constant at a fixed contrast. The source of the signal that changes feed-back gain was decided by the following argument. It is not physically sound to make feed-back gain proportional to contrast, or any other stimulus parameter, unless such a quantity can be extracted from the stimulus by an analogue of a neural network. Thus the gain-changing signal is assumed proportional to one of the signals within the model itself. The gain-changing signal

is chosen here to arise from the d.c. signal present after rectification since it then increases with contrast, and does not vary with time at a fixed contrast, as required.

Deficiencies of the model

There are at least two aspects of Y cell behaviour for which the pooled subunits model cannot account. First, there is the presence of higher response harmonics than the second. Victor & Shapley (1979) showed that there were significant higher harmonics in the Y cell responses they recorded when the stimulus was a grating modulated by a temporal sum of sinusoids. The model we have described cannot produce harmonics any higher than the second. There are at least two alternatives for improving the model in this respect. First, the polynomial used to represent the rectifier could be expanded from second order to higher orders. Secondly, the gain-changing signal in the contrast gain control could be allowed to vary in time rather than assuming the d.c. signal used in the present model; this proposal remains to be tested. Another deficiency in model behaviour can be seen in Figs. 11 and 12: model responses do not advance with increasing contrast as much as do Y cell responses. This failure could not be corrected by a simple adjustment of model parameters. Rather, it suggests that the contrast gain control model used is deficient. Indeed, there are few data in this study with which to test alternative models of the contrast gain control: there are no data, for instance, collected at frequencies other than 2 Hz. The implementation of the contrast gain control used here should therefore be viewed as a rough approximation.

APPENDIX

In what follows, the output of the model for both grating and bar stimuli is calculated. Lower case symbols, such as the time-varying signal $f(t)$, are used to represent scalar quantities and upper case symbols, such as the Fourier component $F(w)$, are used for vector quantities, which have both amplitude and temporal phase. The nth Fourier component is shown as $F(nw)$. All symbols are defined in Fig. 10, or below.

Grating stimulus

Denote the fundamental component of the stimulus

$$L(x,w) = c\cos(2\pi ux - \phi), \tag{11}$$

where c is contrast, u is spatial frequency and ϕ is spatial phase. The output signal from the subunit centre–surround located at $(x_{\text{sub}}, y_{\text{sub}})$ is obtained by weighting the stimulus with the centre–surround's spatial profile, and integrating across space:

$$\begin{aligned} F_D(x_{\text{sub}}, w) &= \int\int_{-\infty}^{\infty} L(x,w)\, D(x, y, x_{\text{sub}}, y_{\text{sub}})\, \mathrm{d}x\, \mathrm{d}y \\ &= \int c\cos(2\pi ux - \phi)\,(\pi^{-\frac{1}{2}} r_{\text{sc}}^{-1} S_{\text{c}} \exp[-(x - x_{\text{sub}})^2 r_{\text{sc}}^{-2}] \\ &\qquad + \pi^{-\frac{1}{2}} r_{\text{ss}}^{-1} S_{\text{s}} \exp[-(x - x_{\text{sub}})^2 r_{\text{ss}}^{-2}])\, \mathrm{d}x \end{aligned}$$

$$= c\cos(2\pi u x_{\text{sub}} - \phi)\int \cos[2\pi u(x - x_{\text{sub}})]\,(\pi^{-\frac{1}{2}} r_{\text{sc}}^{-1} S_{\text{c}} \exp[-(x - x_{\text{sub}})^2 r_{\text{sc}}^{-2}] + \pi^{-\frac{1}{2}} r_{\text{ss}}^{-1} S_{\text{s}} \exp[-(x - x_{\text{sub}})^2 r_{\text{ss}}^{-2}])\,\mathrm{d}x$$

$$= c\cos(2\pi u x_{\text{sub}} - \phi)\,(S_{\text{c}} \exp[-(\pi r_{\text{sc}} u)^2] + S_{\text{s}} \exp[-(\pi r_{\text{ss}} u)^2]). \tag{12}$$

From eqn. (7), the output of the rectifier has a d.c., fundamental and second-harmonic component:

$$\begin{aligned} F_R(x_{\text{sub}}, 0) &= |F_R(x_{\text{sub}}, 2w)|, \\ F_R(x_{\text{sub}}, w) &= F_D(x_{\text{sub}}, w), \\ F_R(x_{\text{sub}}, 2w) &= \tfrac{1}{2} q F_D^2(x_{\text{sub}}, w), \end{aligned} \tag{13}$$

where $||$ represents magnitude. The output of the pool is obtained by weighting the output of each subunit pathway with the pool's spatial profile, and summing across subunits. Since the distance between neighbouring subunits is assumed infinitesimal:

$$F_P(nw) = \int\int_{-\infty}^{\infty} F_R(x_{\text{sub}}, nw)\, P(x_{\text{sub}}, y_{\text{sub}})\,\mathrm{d}x_{\text{sub}}\,\mathrm{d}y_{\text{sub}}.$$

Thus
$$F_P(0) = \int\int |F_R(x_{\text{sub}}, 2w)|\, P(x_{\text{sub}}, y_{\text{sub}})\,\mathrm{d}x_{\text{sub}}\,\mathrm{d}y_{\text{sub}} = |F_P(2w)|. \tag{14}$$

As shown in eqns. (2) and (4), the fundamental component of the pool's signal has the same form as that of a subunit centre–surround, with $r_{\text{sc}}^2 + r_{\text{p}}^2$ replacing r_{sc}^2 and $r_{\text{ss}}^2 + r_{\text{p}}^2$ replacing r_{ss}^2. Making these substitutions in eqn. (12) and setting $x_{\text{sub}} = 0$ (since the middle of the pool is at location zero):

$$F_P(w) = c\cos\phi\,(S_{\text{c}} \exp[-(\pi u)^2(r_{\text{sc}}^2 + r_{\text{p}}^2)] + S_{\text{s}} \exp[-(\pi u)^2(r_{\text{ss}}^2 + r_{\text{p}}^2)]). \tag{15}$$

The pool's second-harmonic component is

$$\begin{aligned} F_P(2w) &= \int\int \tfrac{1}{2} q c^2 \cos^2(2\pi u x_{\text{sub}} - \phi)\,(S_{\text{c}} \exp[-(\pi r_{\text{sc}} u)^2] \\ &\quad + S_{\text{s}} \exp[-(\pi r_{\text{ss}} u)^2])^2\, \pi^{-1} r_{\text{p}}^{-2} \exp[-(x_{\text{sub}}^2 + y_{\text{sub}}^2) r_{\text{p}}^{-2}]\,\mathrm{d}x_{\text{sub}}\,\mathrm{d}y_{\text{sub}} \\ &= \tfrac{1}{4} q c^2 (S_{\text{c}} \exp[-(\pi r_{\text{sc}} u)^2] + S_{\text{s}} \exp[-(\pi r_{\text{ss}} u)^2])^2\, \pi^{-\frac{1}{2}} r_{\text{p}}^{-1} \\ &\qquad \times \int [1 + \cos(4\pi u x_{\text{sub}} - 2\phi)] \exp[-x_{\text{sub}}^2 r_{\text{p}}^{-2}]\,\mathrm{d}x_{\text{sub}} \\ &= \tfrac{1}{4} q c^2 (S_{\text{c}} \exp[-(\pi r_{\text{sc}} u)^2] + S_{\text{s}} \exp[-(\pi r_{\text{ss}} u)^2])^2 \\ &\qquad \times [1 + \cos(2\phi) \exp[-(2\pi r_{\text{p}} u)^2]]. \end{aligned} \tag{16}$$

The output of the complete model is obtained by multiplying pool output by the frequency response of the contrast gain control, and adding the maintained discharge, m, to the d.c. component:

$$\begin{aligned} F_M(0) &= m + F_P(0)\,[1 + g F_P(0)]^{-1}, \\ F_M(w) &= F_P(w)\,(1 + i2\pi\tau w)\,[1 + g F_P(0) + i2\pi\tau w]^{-1}, \\ F_M(2w) &= F_P(2w)\,(1 + i4\pi\tau w)\,[1 + g F_P(0) + i4\pi\tau w]^{-1}. \end{aligned} \tag{17}$$

Several observations can be made from eqns. (15)–(17). (1) The amplitude of the model's fundamental response component varies sinusoidally with the grating's spatial phase. (2) If r_{sc} is small compared with r_{ss} and r_p, the linear component has a spatial resolution given by the radius $\sqrt{(r_{sc}^2+r_p^2)}$, and the second-harmonic component by the radius $\sqrt{2}\, r_{sc}$. Thus, the non-linear component has better spatial resolution. (3) When spatial frequency is high enough, $\exp[-(2\pi r_p u)^2] \ll 1$ and the non-linear component becomes independent of spatial phase.

Bar stimulus

Represent the fundamental component of the stimulus with

$$L(x,w) = \begin{Bmatrix} c & x_b \leqslant x < x_b+b \\ 0 & \text{elsewhere} \end{Bmatrix}, \tag{18}$$

where c is contrast, x_b is the location of the left side of the bar, and b is bar width. The signals at successive stages of the model can be derived by similar arguments to those used for the grating stimulus.

Output of the subunit centre–surround:

$$F_D(x_{sub}, w) = c[S_c\ \mathrm{erfb}(x_b - x_{sub}, b, r_{sc}) + S_s\ \mathrm{erfb}(x_b - x_{sub}, b, r_{ss})], \tag{19}$$

where

$$\mathrm{erfb}(x,b,r) = \mathrm{erf}[\sqrt{2}\,(x+b)/r] - \mathrm{erf}(\sqrt{2}\,x/r);\ \mathrm{erf}(x) = (2\pi)^{-\frac{1}{2}}\int_0^x \exp[-\tfrac{1}{2}z^2]\,dz. \tag{20}$$

Pool output:

$$F_P(0) = |F_P(2w)|,$$

$$F_P(w) = c[S_c\ \mathrm{erfb}(x_b, b, \sqrt{(r_{sc}^2+r_p^2)}) + S_s\ \mathrm{erfb}(x_b, b, \sqrt{(r_{ss}^2+r_p^2)})],$$

$$F_P(2w) = \tfrac{1}{2}qc^2(2\pi)^{-\frac{1}{2}}\int_{-\infty}^{\infty} [S_c\ \mathrm{erfb}(x_b - r_p z/\sqrt{2}, b, r_{sc}) + S_s\ \mathrm{erfb}(x_b - r_p z/\sqrt{2}, b, r_{ss})]^2 \exp[-\tfrac{1}{2}z^2]\,dz. \tag{21}$$

(The last equation involves integrals of the squared error function and is best left in the form shown.)

Model output: as in eqn. (17).

We thank L. J. Frishman for her help with the experiments, H. R. Wilson for his suggestions regarding experimental design, and B. G. Cleland, J. G. Robson and R. M. Shapley for their comments on the manuscript. This work was supported by grants F05 TW03177 from the Fogarty International Center and R01 EY00206 from the National Eye Institute of the U.S. National Institutes of Health.

REFERENCES

CLELAND, B. G. (1983). Centre and surround properties of the receptive fields of X and Y ganglion cells in the cat retina. *Proceedings of the Australian Physiological and Pharmacological Society* **14**, 192–201.

CLELAND, B. G., DUBIN, M. W. & LEVICK, W. R. (1971). Sustained and transient neurones in the cat's retina and lateral geniculate nucleus. *Journal of Physiology* **217**, 473–496.

CLELAND, B. G. & ENROTH-CUGELL, C. (1966). Cat retinal ganglion cell responses to changing light intensities: sinusoidal modulation in the time domain. *Acta physiologica scandinavica* **68**, 365–381.

CLELAND, B. G., HARDING, T. H. & TULUNAY-KEESEY, U. (1979). Visual resolution and receptive field size: examination of two kinds of cat retinal ganglion cell. *Science* **205**, 1015–1017.

CLELAND, B. G. & LEVICK, W. R. (1974). Brisk and sluggish concentrically organized ganglion cells in the cat's retina. *Journal of Physiology* **240**, 421–456.

DERRINGTON, A. M. & LENNIE, P. (1982). The influence of temporal frequency and adaptation level on receptive field organization of retinal ganglion cells in cat. *Journal of Physiology* **333**, 343–366.

ENROTH-CUGELL, C., HERTZ, B. G. & LENNIE, P. (1977). Cone signals in the cat's retina. *Journal of Physiology* **269**, 273–296.

ENROTH-CUGELL, C. & ROBSON, J. G. (1966). The contrast sensitivity of retinal ganglion cells of the cat. *Journal of Physiology* **187**, 517–552.

ENROTH-CUGELL, C., ROBSON, J. G., SCHWEITZER-TONG, D. E. & WATSON, A. B. (1983). Spatio-temporal interactions in cat retinal ganglion cells showing linear spatial summation. *Journal of Physiology* **341**, 279–307.

FREEMAN, A. W. & ENROTH-CUGELL, C. (1985). Receptive field spatial structure of cat retinal Y cells. *Investigative Ophthalmology and Visual Science* **26**, suppl., 263.

FRISHMAN, L. J. & LINSENMEIER, R. A. (1982). Effects of picrotoxin and strychnine on non-linear responses of Y-type cat retinal ganglion cells. *Journal of Physiology* **324**, 347–363.

HOCHSTEIN, S. & SHAPLEY, R. M. (1976*a*). Quantitative analysis of retinal ganglion cell classifications. *Journal of Physiology* **262**, 237–264.

HOCHSTEIN, S. & SHAPLEY, R. M. (1976*b*). Linear and nonlinear spatial subunits in Y cat retinal ganglion cells. *Journal of Physiology* **262**, 265–284.

LINSENMEIER, R. A., FRISHMAN, L. J., JAKIELA, H. G. & ENROTH-CUGELL, C. (1982). Receptive field properties of X and Y cells in the cat retina derived from contrast sensitivity measurements. *Vision Research* **22**, 1173–1183.

NIKARA, T., BISHOP, P. O. & PETTIGREW, J. D. (1968). Analysis of retinal correspondence by studying receptive fields of binocular single units in cat striate cortex. *Experimental Brain Research* **6**, 353–372.

PEICHL, L. & WÄSSLE, H. (1979). Size, scatter and coverage of ganglion cell receptive field centres in the cat retina. *Journal of Physiology* **291**, 117–141.

SHAPLEY, R. & ENROTH-CUGELL, C. (1984). Visual adaptation and retinal gain controls. *Progress in Retinal Research* **3**, 263–343.

SHAPLEY, R. M. & VICTOR, J. D. (1978). The effect of contrast on the transfer properties of cat retinal ganglion cells. *Journal of Physiology* **285**, 275–298.

SHAPLEY, R. M. & VICTOR, J. D. (1981). How the contrast gain control modifies the frequency responses of cat retinal ganglion cells. *Journal of Physiology* **318**, 161–179.

SO, Y. T. & SHAPLEY, R. (1979). Spatial properties of X and Y cells in the lateral geniculate nucleus of the cat and conduction velocities of their inputs. *Experimental Brain Research* **36**, 533–550.

VICTOR, J. D. & SHAPLEY, R. M. (1979). The nonlinear pathway of Y ganglion cells in the cat retina. *Journal of General Physiology* **74**, 671–689.

WIESEL, T. N. (1960). Receptive fields of ganglion cells in the cat's retina. *Journal of Physiology* **153**, 583–594.